BRAIN
ORIGINAL ARTICLE

Inactivating *Celsr2* promotes motor axon fasciculation and regeneration in mouse and human

Quan Wen,[1,†] Huandi Weng,[1,†] Tao Liu,[1] Lingtai Yu,[1] Tianyun Zhao,[2] Jingwen Qin,[2] Si Li,[3,4] Qingfeng Wu,[3,4] Fadel Tissir,[5,6] Yibo Qu[1,7,8] and Libing Zhou[1,8,9,10]

†These authors contributed equally to this work.

See Petrova and Hakim (https://doi.org/10.1093/brain/awac021) for a scientific commentary on this article.

Understanding new modulators of axon regeneration is central to neural repair. Our previous work demonstrated critical roles of atypical cadherin *Celsr2* during neural development, including cilia organization, neuron migration and axon navigation. Here, we address its role in axon regeneration.

We show that *Celsr2* is highly expressed in both mouse and human spinal motor neurons. *Celsr2* knockout promotes axon regeneration and fasciculation in mouse cultured spinal explants. Similarly, cultured *Celsr2* mutant motor neurons extend longer neurites and larger growth cones, with increased expression of end-binding protein 3 and higher potassium-induced calcium influx. Mice with *Celsr2* conditional knockout in spinal motor neurons do not exhibit any behavioural deficits; however, after branchial plexus injury, axon regeneration and functional forelimb locomotor recovery are significantly improved. Similarly, knockdown of *CELSR2* using shRNA interference in cultured human spinal motor explants and motor neurons increases axonal fasciculation and growth. In mouse adult spinal cord after root avulsion, in mouse embryonic spinal cords, and in cultured human motor neurons, *Celsr2* downregulation is accompanied by increased levels of GTP-bound Rac1 and Cdc42, and of JNK and c-Jun.

In conclusion, Celsr2 negatively regulates motor axon regeneration and is a potential target to improve neural repair.

1 Guangdong-Hongkong-Macau Institute of CNS Regeneration, Ministry of Education CNS Regeneration Collaborative Joint Laboratory, Jinan University, Guangzhou 510632, P. R. China
2 Department of Anesthesiology, Guangzhou Women and Children's Medical Center, Guangzhou Medical University, Guangzhou, P. R. China
3 State Key Laboratory of Molecular Development Biology, Institute of Genetics and Developmental Biology, Chinese Academy of Sciences, Beijing 100101, P. R. China
4 University of Chinese Academy of Sciences, Beijing 100101, P. R. China
5 Institute of Neuroscience, Developmental Neurobiology, Université Catholique de Louvain, Brussels, Belgium
6 College of Health and Life Sciences, Hamad Bin Khalifa University (HBKU), Doha, Qatar
7 Guangdong-Hong Kong-Macao Greater Bay Area Center for Brain Science and Brain- Inspired Intelligence, Guangzhou 510515, P. R. China
8 Co-innovation Center of Neuroregeneration, Nantong University, Jiangsu, P. R. China
9 Bioland Laboratory (Guangzhou Regenerative Medicine and Health Guangdong Laboratory), Guangzhou 510005, P. R. China
10 Department of Neurology and Stroke Center, The First Affiliated Hospital of Jinan University, Guangzhou 510632, P. R. China

Received March 18, 2021. Revised July 20, 2021. Accepted July 26, 2021. Advance access publication January 4, 2022

Correspondence to: Libing Zhou
Guangdong-Hongkong-Macau Institute of CNS Regeneration, Jinan University
Huangpu Avenue West 601, Guangzhou 510632, P.R. China
E-mail: tlibingzh@jnu.edu.cn

Correspondence may also be addressed to: Yibo Qu
E-mail: tquyibo@jnu.edu.cn

Keywords: axon regeneration; spinal motor neurons; brachial plexus injury; root avulsion; human embryos

Abbreviations: cKO = conditional knockout; DIV = days *in vitro*; NMJ = neuromuscular junction; WPC = week post conception

Introduction

Spinal motor neurons are unique as their somas and dendrites reside in the CNS, but their axons extend in the PNS, giving them qualities of both CNS and PNS neurons. Following injury, spinal motor axons regenerate better than those of premotor CNS neurons.[1,2] Brachial plexus injury often leads to root avulsion and lesions of motor neurons and axons, with dramatic consequences, and represents an important health issue. Root lesions interrupt corresponding segmental motor axons and sensory fibres, leading to axon degeneration and, eventually, the death of motor neurons.[3] Contrary to distal motor axon injuries, axons regenerate poorly after root avulsion. Reimplantation of avulsed roots in the spinal cord provides a scaffold that may facilitate survival of injured motor neurons and regeneration of their axons.[4] These observations resulted in the development of a surgical method to restore function after root injury.[5] Potential therapies to promote axon regrowth and functional recovery have been considered.[6,7] Yet, the limits of current treatments underscore the need for further basic research into mechanisms that enhance motor axon regeneration.[8]

Together with its two paralogues Celsr1 and Celsr3, the atypical cadherin Celsr2 is an orthologue of the *Drosophila* planar cell polarity (PCP) protein Flamingo. Celsr1–3 play critical roles during brain development.[9,10] Genetic studies in mice showed that Celsr2 and Celsr3 regulate axonal pathfinding, motor neuron migration, and ependymal ciliogenesis,[11–14] whereas mutant phenotypes suggest that Celsr2 and Celsr3 act synergistically, they were also reported to play opposite roles in steering neurite outgrowth *in vitro*.[15]

Motor axon phenotypes in *Celsr3* and *Celsr2* double mutant mice[14] have also been observed in mice with *Fzd3* knockout[16] and upon motor neuron-specific inactivation of *Rac1*,[17] hinting at a mechanistic link between Celsr2 and 3, Fzd3 and GTPase-dependent regulation of growth cone extension. Contrary to *Celsr3*, the expression of which is sharply downregulated after birth, *Celsr2* expression remains high in the adult CNS.[18] This prompted us to investigate whether Celsr2 has any effect on the regeneration of injured motor axons.

To address this, we compared motor axon outgrowth in control and *Celsr2*-deficient spinal cord explants and cultured motor neurons from mouse and human embryos. Human *CELSR2* was downregulated using a lentivirus encoding *Celsr2* shRNA, whereas mouse *Celsr2* was inactivated genetically. To investigate the role of Celsr2 during adult motor axon regeneration, we performed spinal root avulsion and motor root reimplantation in control and *Celsr2* motor neuron-specific knockout mice, and evaluated axon regeneration and functional recovery after surgery.

Materials and methods

Animals

Animal procedures were performed following recommendations in the Guide for the Care and Use of Laboratory Animals of the National Institutes of Health. The protocol was approved by the Laboratory Animal Ethics Committee at Jinan University (permit number: 20111008001). The generation of $Celsr2^{-/-}$ and $Celsr2^{LacZ}$ mice was described previously.[13] *Isl1-Cre; Celsr2*$^{f/-}$ conditional knockout animals (*Celsr2* cKO) were obtained by crossing $Celsr2^{-/-}$ with *Isl1-Cre* mice (Stock No: 024242, Jackson Laboratory) to generate *Isl1-Cre;* $Celsr2^{+/-}$ mice, which were mated with $Celsr2^{f/f}$ mice. To stage embryos, animals were mated in the afternoon and vaginal plugs were checked on the next morning, noted as embryonic Day 0.5 (E0.5).

Human embryonic samples

Human embryos were collected following drug-induced abortions at Guangzhou Women and Children's Medical Center. All procedures were approved by the Medical Ethics Committees of the hospital (ref. file 2016041303) and in agreement with the Helsinki Convention. Informed consent was obtained from both parents and pregnant women had no reported disease history. Embryos were transferred into culture medium (DMEM-F12 plus 50 U/ml penicillin–streptomycin) immediately after expulsion. The age was estimated by the date of the mother's last menstruation, and by measurement of crown rump length, according to a growth chart,[19] and is expressed as weeks post conception (WPC).

Motor neuron explant culture and analysis of axon growth

Mouse embryonic motor neuron explant culture was performed as described.[20] Briefly, cervical spinal motor neuron explants from E13.5 $Celsr2^{+/+}$ (control) and $Celsr2^{-/-}$ embryos were minced and cultured on coverslips coated with polylysine (0.75 μg/cm^2, BD, Biocoat) and laminin (0.9 μg/cm^2), in 24-well plates (Corning). Plates were kept at room temperature for 30 min to allow explants to attach, and then transferred to a cell culture incubator. The culture medium consisted in neurobasal medium (Invitrogen) supplemented with 2% (vol/vol) B27 (Invitrogen), 50 U/ml penicillin–streptomycin, 2 mM L-glutamine and 20 ng/ml BDNF (R&D Systems). In each group (control and *Celsr2* mutant), three E13.5 litters of five to seven embryos were used and 19–22 explants were suitable for analysis. Human spinal motor neuron explant culture was performed from seven post conceptional weeks (WPC7) embryos, in 12-well plates, using similar procedures. After 24-h culture, 2×10^9 transduction units (TU)/ml lentivirus

encoding CELSR2-shRNA, or CELSR2 scrambled shRNA as control was added to the culture medium and replaced by fresh culture medium after 48 h. After 6 days *in vitro* (DIV) for mouse and 5 DIV for human, cultured explants were fixed and immunostained with anti-Tuj1 (1:1000; ab18207; Abcam) and anti-choline acetyl transferase (ChAT; 1:500 dilution; AB144P, Millipore) antibodies. The maximal area covered by growing axons was estimated using ImageJ.[21] In each explant, four axes (eight directions in total) were drawn with the explant at the centre; the maximal axon length was measured in each direction and the average was calculated. To evaluate fasciculation, axonal bundles with diameters larger than 8 μm were counted in the region 150–200 μm away from the explant surface.[22]

Primary spinal motor neuron culture and analysis

Ventral horns of cervical spinal cords from E13.5 mouse or WPC7–8 human embryos were dissected out in cold DPBS (Dulbecco's PBS without Ca^{2+} and Mg^{2+} at pH 7.4). After trypsinization (0.5% trypsin, Gibco) and cell counting, isolated cells (2.5×10^3 cells/cm^2) were seeded on polylysine- and laminin-coated coverslips, in 12-well plates, and cultured in neurobasal medium (Invitrogen) plus 2% B27, 20 ng/ml BDNF, 50 U/ml penicillin–streptomycin and 2 mM L-glutamine. Half of the medium was replaced by fresh medium every 2–3 days. To estimate the effects of *CELSR2* inactivation in human spinal neurons, lentivirus (2×10^9 TU/ml) encoding CELSR2-shRNA, or CELSR2 scrambled shRNA as control was added to the culture medium after 1 DIV, and fresh culture medium was added 48 h later. After 5 DIV, cells were fixed and stained with mouse anti-Tuj1 (1:1000; ab18207; Abcam) and TexRed-Phalloidin (1:50, Life Technologies Corporation). Neurite length and growth cone areas were measured using Imaris and ImageJ. Data were collected from at least three independent cultures, and a total of 50–60 neurons were used for quantification in each group.

Measurement of intracellular calcium

After 16 DIV for mouse and 19 DIV for human, cultured neurons were washed three times with Hank's balance salt solution (HBSS), incubated in complete medium supplemented with 5 μM Fura-4 AM (DOJINDO Chemical Technology) for 30 min and rinsed with HBSS. Cover slips were transferred to a culture chamber under an inverted microscope (Axioplan 2; Zeiss) and perfused with calcium-imaging buffer at a rate of 2.0 ml/min for 13 min. KCl (50 mM) was applied to stimulate calcium influx. Fluorescence density was analysed to estimate the intracellular calcium peak using ImageJ software. Three litters (six to seven embryos in each litter) of E13.5 mouse embryos and three human embryos (two at WPC7 and one at WPC8) were used for spinal neuron culture.

Root avulsion/reimplantation surgery

Adult (2–3 months old, 24–28 g) *Celsr2* cKO ($n = 12$) and *Celsr2*$^{f/-}$ (control; $n = 12$) mice were selected for surgery and anaesthetized with avertin (1.25%, 20 μl/g, intraperitoneal injection). C5–C7 spinal segments were exposed under an operating microscope following unilateral hemilaminectomy. Right C5–C7 dorsal and ventral roots were dissected out; 2–3 mm of spinal roots in segments of C5 and C7 were removed to prevent reconnection to spinal cord, and the right C6 ventral root was reimplanted to its initial location. During the operation, a thermostatic surgical pad was used to maintain normal body temperature. After the procedure, animals were housed in individual cages. They resumed drinking and eating within 24 h and recovered uneventfully. Males and females were used indiscriminately. At Day 1 after surgery, animals without complete paralysis of right forelimbs were excluded and the rest were proceeded for dynamic behavioural tests (below) up to 56 days. Subsequently, animals were perfused and samples were collected after EMG recording.

Behavioural tests

Behavioural tests were carried out by an experimenter blind to mouse genotypes.

Grooming test

C6 spinal motor axons travel in musculocutaneous nerve and innervate the biceps to control elbow flexion. Functional recovery was assessed by the grooming test[23] and the scores were determined by monitoring the position that the right forelimb could reach. After water was sprayed on the animal's head, the forelimb movements were recorded for 2 min with a video camera and the scores were given as described.[24] After 24 h of surgery, successful animals had scores of 0, and those with scores above 0 were excluded.

Climbing tests

Climbing tests evaluated the usage of forelimbs.[25,26] Briefly, mice were placed in a clear Perspex cylinder (170 mm in height, 90 mm in diameter) and the times the forelimb touched the wall were counted during a video recording. The ratio of hits by forelimbs on the operated versus control side was calculated.

EMG recording

The musculocutaneous nerve and biceps brachii were exposed under a surgical microscope under 1.25% avertin anaesthesia. A stimulating electrode was placed on the musculocutaneous nerve and a bipolar recording electrode was inserted in the centre of the biceps, with a grounding electrode in the subcutaneous tissue. Similar stimulations (30 μA, 30 ms) were applied in all animals. EMG signals were collected with a multichannel system (VikingQuest EMG/EP System, Nicolet). Individual responses were measured six times, at 2-min intervals, on left and right sides, and the mean from six trials represented one sample. The peak-to-peak amplitude of evoked potentials was measured and expressed as the ratio between the operated (R) and the unoperated (L) sides. After recording, the biceps brachii were fixed in 4% paraformaldehyde to estimate the R/L weight ratio.

Histology and immunohistochemistry

C5–C7 spinal segments or musculocutaneous nerve were cut into 15-μm frozen sections for immunostaining. The blocking buffer was composed of 5% goat serum and 3% bovine serum albumin diluted in 0.1 M PBS. Signal was detected with Alexa Fluor 546 or 488 coupled secondary antibodies (1:1000, Invitrogen). Primary antibodies were: goat anti-ChAT (1:500, ab144p, Millipore), chicken anti-β-gal (1:500, ab9361, Abcam), rabbit anti-Isl1 (1:1000, Abcam) and goat anti-human CELSR2 (1:100, AF6379, R&D systems). To visualize neuromuscular junctions (NMJs), the biceps were collected 50 days post-surgery and the wet weight was recorded. Seventy-micrometre horizontal sections were prepared with a sliding microtome (Leica, Germany) and double stained with rabbit anti-NF200 (1:500, n4142, Sigma) and α-BT (1:1000, Molecular probes). To analyse axon number in musculocutaneous nerves, tissues were fixed with 2.5% glutaraldehyde plus 2% paraformaldehyde and 500-nm semi-thin sections were stained

with 1% Toluidine Blue; images were taken under a 63× oil objective.

Electron microscopy

Animals were perfused with 2.5% glutaraldehyde plus 2% paraformaldehyde 56 days after root avulsion/reimplantation. Segments (2–3 mm) of musculocutaneous nerves adjacent to biceps were collected for post-fixation at 4°C overnight. After washing in phosphate buffer, samples were immersed in 0.5% osmic acid, dehydrated in ethanol and embedded in resin (EMbed 812, Electron Microscope Sciences). Semi-thin (500-nm) transverse sections were stained with 1% Toluidine Blue and images were captured under a 63× oil objective. For ultrastructural analysis, 50-nm ultrathin sections were prepared for lead staining and the images were captured using a Philips 400 transmission electron microscope.

Rac1/Cdc42 activity assay

Levels of GTP-bound Cdc42 and Rac1 proteins of E13.5 mouse samples containing cervical spinal motor neurons, 5-DIV cultured human spinal motor neurons and C5–C7 ventral horns of adult animals 3 days after surgery were estimated using a Rac1/Cdc42 Activation Assay Kit (#17–441, Merck Millipore). Briefly, samples were homogenized in the lysis buffer (125 mM HEPES (pH 7.5), 750 mM NaCl, 5% Igepal CA-630, 50 mM $MgCl_2$, 5 mM EDTA, 10% glycerol and protease inhibitors). Lysates were incubated with glutathione-agarose beads conjugated with the PAK1 Protein Binding Domain fused to GST (GST-PBD) at 4°C for 60 min and the beads were washed three times in lysis buffer. GTP-bound proteins were eluted in sample gel buffer and subjected to western blots.

Western blots

Protein extracts from E13.5 mouse cervical segments, C5–C7 ventral horns of adult animals 3 days after surgery, 5-DIV cultured human motor neuron explants and proteins eluted from glutathione-agarose beads were analysed on 10% SDS polyacrylamide gels and then transferred to 0.45-μm nitrocellulose membranes. The following primary antibodies were used: anti-β-tubulin (Tuj1) rabbit polyclonal antibody (1:1000; ab18207, Abcam), anti-GAPDH mouse polyclonal antibody (1:1000; ab8245, Abcam), anti-JNK rabbit polyclonal antibody (1:1000; 9252, CST), anti-c-Jun rabbit polyclonal antibody (1:1000; 3270S, CST), anti-EB3 rat polyclonal antibody (1:1000; ab53360, Abcam), anti-GSK-3β polyclonal antibody (1:1000; 9315, CST), anti-Rac1 mouse polyclonal antibody (1:1000; 610650, BD Pharmingen), anti-CDC42 rabbit polyclonal antibody (1:1000; 11A11, CST), goat anti-human CELSR2 (1:1000, AF6379, R&D systems); the secondary antibodies include peroxidase anti-rabbit IgG (1:5000, ab6721, Abcam) and peroxidase anti-mouse IgG (1:10 000; Vector Laboratories). Immunoreactivity was detected using an enhanced chemiluminescence detection kit (1705061, Bio-Rad).

Statistical analysis

Data are presented as mean ± SEM. Results of behavioural tests were analysed with two-way ANOVA; receptor clusters with axon terminal overgrowth were compared using chi-square; and other comparisons were made using Student's t-test of two-independent samples. The cell count and fluorescence density were assessed using ImageJ software.

Data availability

The data that support the findings of this study are available from the corresponding authors upon reasonable request.

Results

Celsr2 is strongly expressed in spinal motor neurons

To study Celsr2 expression, we used *Celsr2*$^{LacZ/+}$ mice, in which an internal ribosomal entry site (IRES) and the *LacZ* gene are inserted into *Celsr2* exon 23.[13] When Celsr2-expressing cells were visualized by anti-β-gal staining, signal was found in several cell types (Fig. 1A and F). In E12.5 spinal sections, all Isl1-positive cells in the ventral horn co-expressed β-gal (Fig. 1A–E). In adult spinal sections, motor neurons were positive using anti-ChAT immunostaining and all of them were also positive for β-gal (Fig. 1F–J). In WPC8 human spinal sections, double immunostaining showed that most ISL1-positive cells were also positive for CELSR2 in the ventral horn (Fig. 1K–O). Expression of CELSR2 is maintained in adult human spinal cord (GTEx Human brain RNA-Seq dataset, https://www.proteinatlas.org/ENSG00000143126-CELSR2/brain). Thus, Celsr2 is expressed in mouse and human spinal motor neurons.

Inactivating *Celsr2* promotes axon growth and fasciculation in cultured mouse spinal motor explants

To assess the role of Celsr2 in motor axon regeneration, we used spinal motor neuron explant cultures.[20] Cervical spinal explants containing motor neurons were prepared from E13.5 *Celsr2*$^{-/-}$ and control embryos and cultured for 6 DIV (Fig. 2A). Cells and outgrowing axons expressed ChAT in both groups (Fig. 2B and E), indicating that they corresponded to spinal motor neurons from the ventral column. Anti-Tuj1 signal co-localized extensively with ChAT-immunoreactivity (Fig. 2C, D, F and G). In Tuj1-immunostained preparations, the maximal area covered by growing axons and axonal length (indicated in Fig. 2A) were significantly increased in *Celsr2*$^{-/-}$ mutant compared with control samples (Fig. 2H and I; three litters of embryos in each group, five to seven embryos in each litter, 19 and 22 explants in mutant and control, respectively; $P < 0.05$ and 0.01). In addition, larger axonal bundles were formed in the mutant explants (Fig. 2C and F, insets). In the region 150–200 μm away from explant borders, the number of large (>8 μm) axon bundles, estimated as described,[22] was significantly higher in mutant explants (Fig. 2J; $P < 0.001$). Together, these results suggest that inactivation of *Celsr2* stimulates spinal motor axon growth and fasciculation.

Celsr2 inactivation contributes to cytoskeleton organization in growth cones of cultured mouse spinal motor neurons

In explant cultures, spinal motor neurons are intermingled with other cells such as interneurons or glial cells that may influence motor axon growth. To check whether Celsr2 acted in a cell-autonomous manner, we cultured isolated motor neurons from E13.5 embryos. After 6 DIV, axons were readily identified by anti-Tuj1 immunofluorescent staining (Fig. 3A and B). As in the explant cultures, the total neurite length was significantly enhanced in the mutants (Fig. 3E; three independent experiments, 35 neurons and 41 neurons in the mutant and control, respectively; $P < 0.0001$). The growth cone size, estimated by F-actin immunostaining (Fig. 3C and D), was increased in mutant compared to control

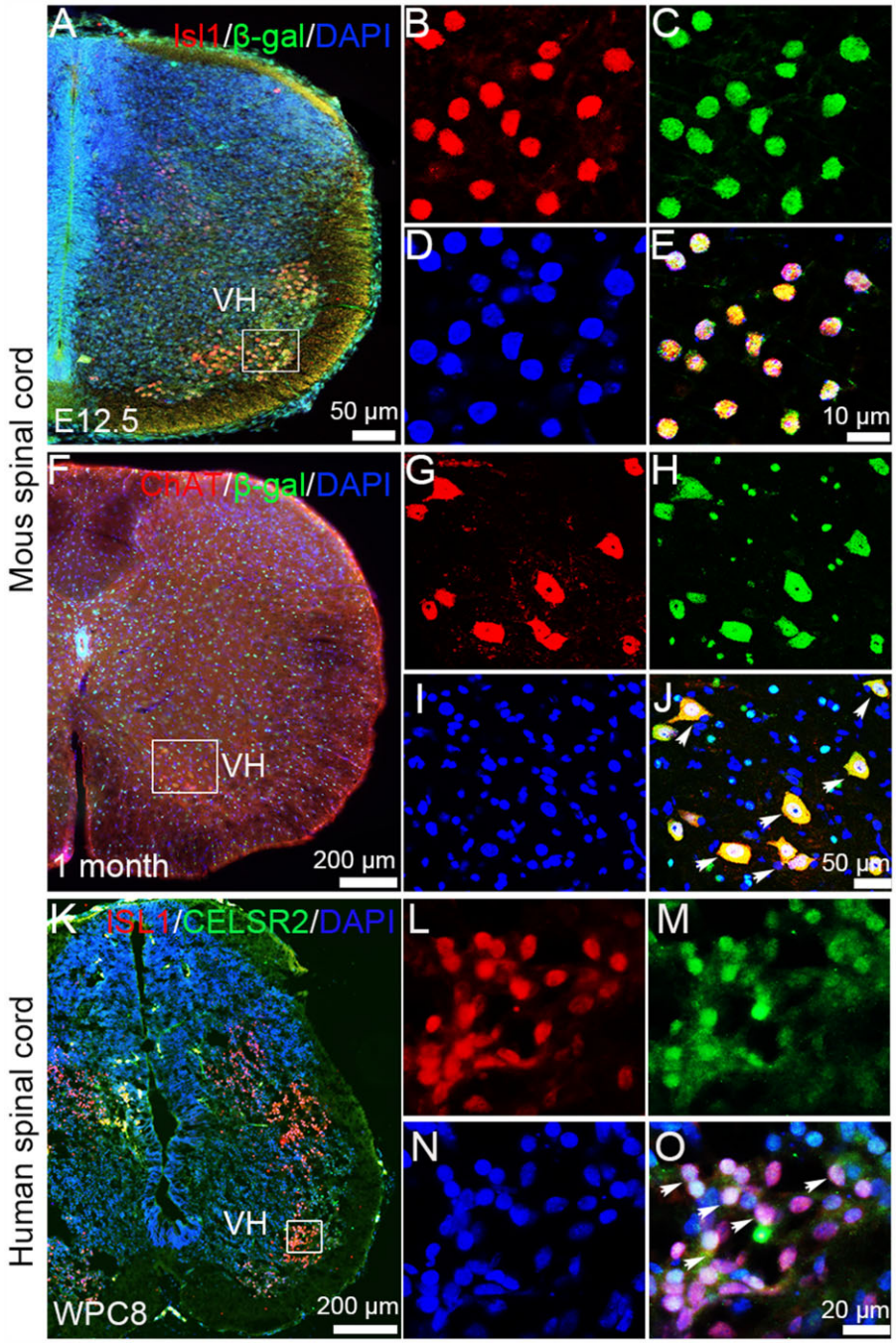

Figure 1 *Celsr2* expression is enriched in mouse and human spinal motor neurons. Using *Celsr2*^{LacZ} transgenic mice, Celsr2 expression is detected by anti-β-gal immunostaining. (**A–E**) E12.5 spinal sections were immunostained for Isl1 (red), β-gal (green) and counterstained for DAPI (blue). The merged image showed that all Isl1-positive cells in the ventral horn (VH) co-labelled by β-gal immunoreactivity (**E**). (**F–J**) In adult spinal sections, all ChAT-positive (red) spinal motor neurons co-expressed β-gal (green) indicated by arrows (**J**). (**K–O**) In WPC8 human spinal sections, ISL1 and CELSR2 double immunofluorescent staining showed that CELSR2 was expressed in ISL1-positive neurons in the ventral horn (VH) indicated by arrows (**O**). **B–E**, **G–J** and **L–O** correspond to boxed areas in **A**, **F** and **K**, respectively. Nuclei were counterstained by DAPI (blue).

samples (Fig. 3F; three independent experiments, 39 neurons and 55 neurons in the mutant and control, respectively; $P < 0.0001$).

Axonal growth is a dynamic process that requires remodelling of the cytoskeleton. The upregulation of the microtubule plus end-binding protein 3 (EB3) is an index of axon regeneration.[27] We analysed E13.5 spinal ventral horn extracts by western blots and found that the EB3 levels were markedly higher in *Celsr2*$^{-/-}$ than in controls (Fig. 3G). Intracellular calcium is an established indicator of cytoskeleton reorganization during axon growth.[28] In 16-DIV cultured spinal motor neurons, we studied potassium-stimulated calcium influx using the calcium sensitive dye Fura-4 AM (Supplementary Fig. 1A). Fluorescent intensity of cultured neurons measured before and after potassium stimulation showed a significant increase of intracellular calcium peak in *Celsr2*$^{-/-}$ compared to control neurons (Supplementary Fig. 1B and C; $P < 0.05$).

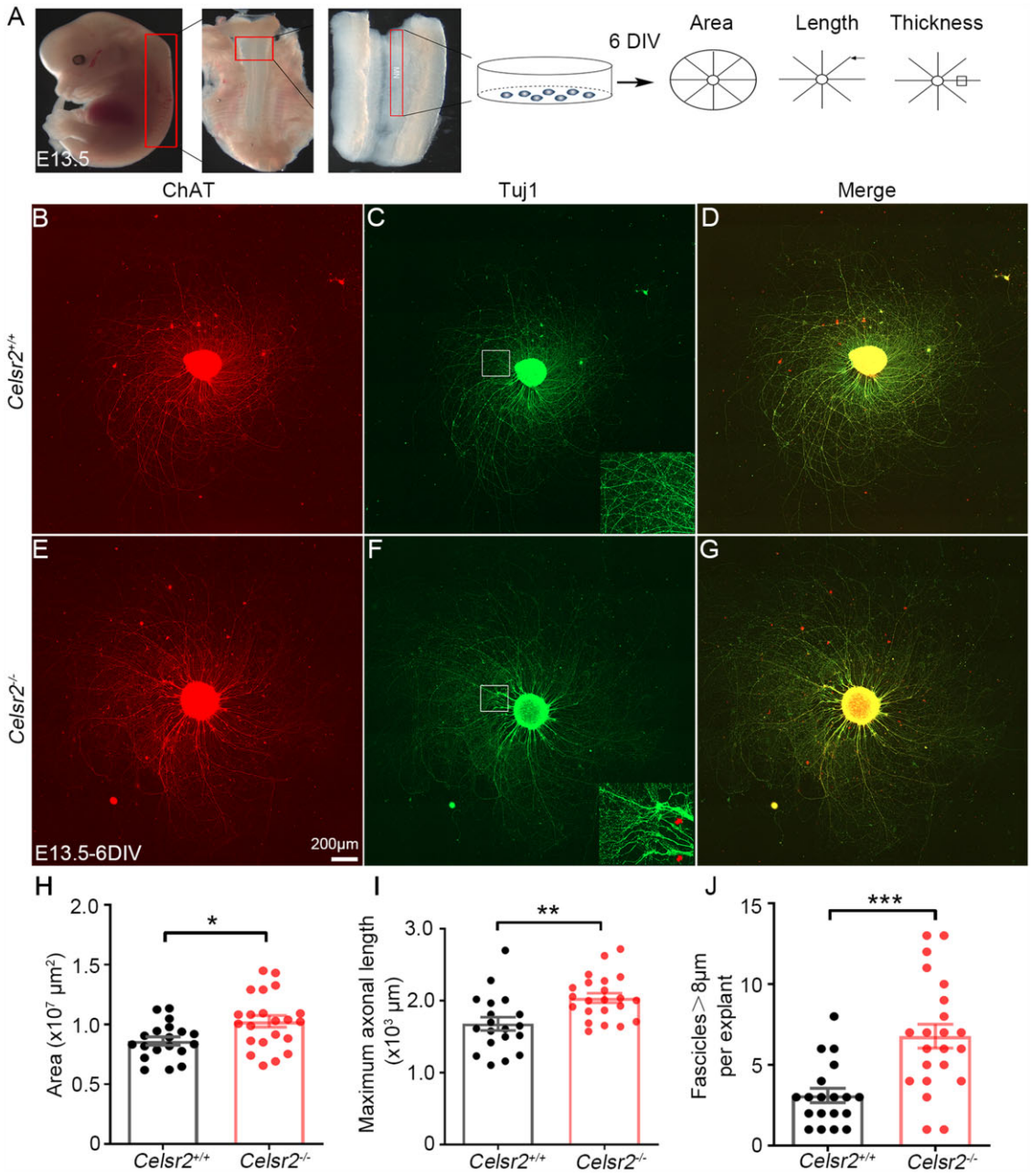

Figure 2 *Celsr2* knockout improves axon growth in mouse spinal motor explant culture. (**A**) Schema of the experimental procedure for explant culture and analysis. (**B–G**) Spinal motor neuron explants from E13.5 *Celsr2*$^{+/+}$ (**B–D**) and *Celsr2*$^{-/-}$ mouse embryos (**E–G**) were cultured for 6 DIV and then immunostained for ChAT (**B** and **E**; red) and Tuj1 (**C** and **F**; green). Both signals co-localize (**D** and **G**; yellow). Representative axonal bundles are indicated in the insets of **C** and **F**. (**H–J**) Quantification of the maximal area covered by growing axons in 10^7 μm^2 (**H**; control: 0.86 ± 0.03, mutant: 1.02 ± 0.05; $P < 0.05$), maximal axon length in 10^3 μm (**I**; control: 1.68 ± 0.09, mutant: 2.04 ± 0.07; $P < 0.001$) and number of large axon bundles (>8 μm in diameter; **J**; control: 3.11 ± 0.45, mutant: 6.77 ± 0.74; $P < 0.001$). These parameters are increased significantly in the mutant compared to the control. ***$P < 0.001$; **$P < 0.01$; *$P < 0.05$; Student's *t*-test; $n = 19$ in the control and $n = 22$ in the mutant.

Celsr2 conditional knockout animals harbour improved axonal regeneration and functional recovery after root avulsion/reimplantation

To test whether *Celsr2* influences regeneration of adult motor axons *in vivo*, we first generated *Celsr2* cKO mice with conditional inactivation of *Celsr2* in spinal motor neurons by *Isl1-Cre* according to previous reports,[14,29,30] and confirmed that *Celsr2* mRNA was absent in spinal motor neurons using *in situ* hybridization (Supplementary Fig. 2). These animals develop to adulthood unremarkably, without apparent neurological deficit. We next carried out C5–C7 root avulsion and C6 motor root reimplantation as described.[24] In this model, upon reimplantation of root C6, regenerating axons could reinnervate the biceps brachii and restore partial function,[31] which can be evaluated by monitoring elbow flexion in grooming and climbing tests. In both tests, *Celsr2* cKO animals showed a significantly improved recovery of injured right forelimb function compared with littermate controls (*Celsr2*$^{f/-}$; Fig. 4A and B). Inactivation of *Celsr2* in motor neurons also decreased biceps atrophy, as evidenced by increased muscle wet weight (Fig. 4C and D), fostered biceps reinnervation with formation of new NMJs, as indicated by more numerous NMJs (Fig. 4F;

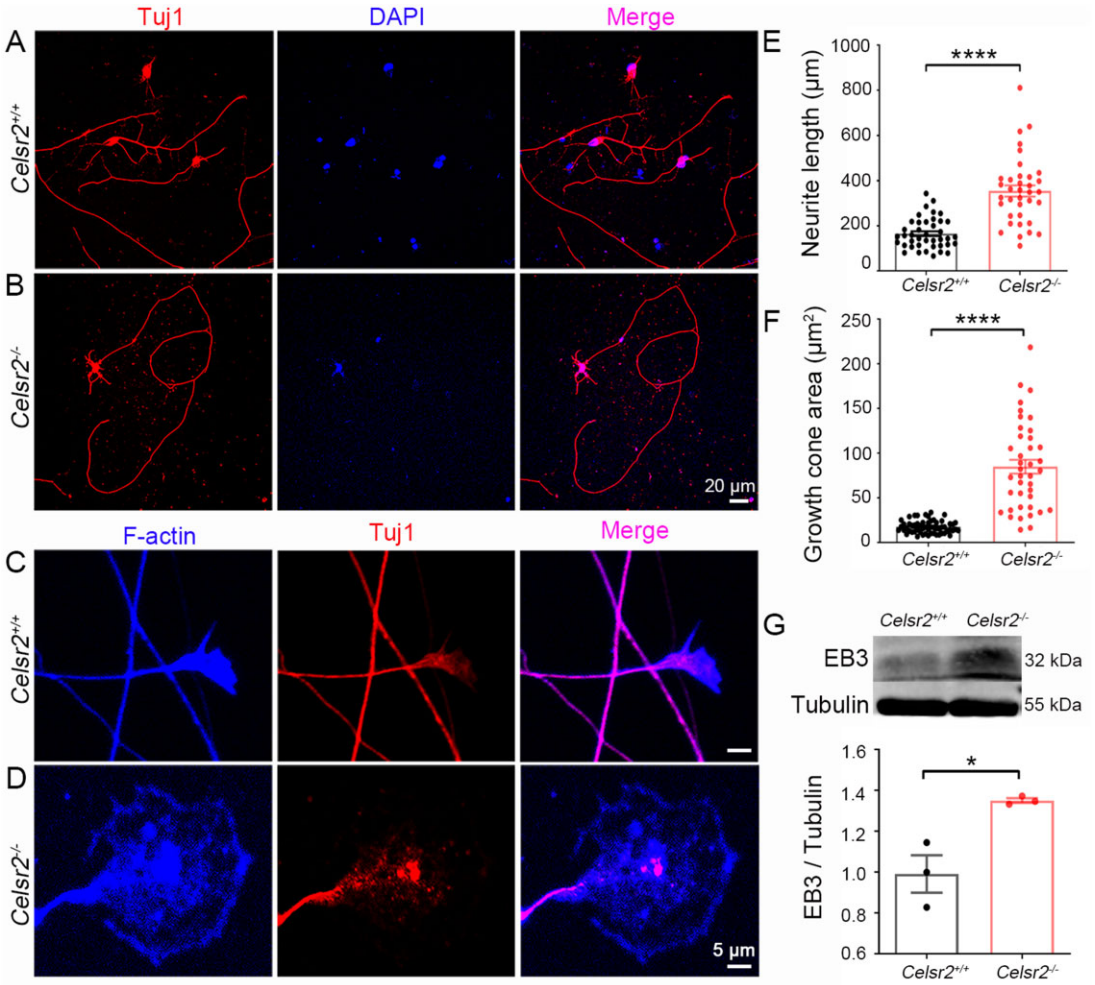

Figure 3 *Celsr2* knockout contributes to neurite growth in primary spinal motor neuron culture. (**A** and **B**) E13.5 spinal motor neurons from *Celsr2*$^{+/+}$ (**A**) and *Celsr2*$^{-/-}$ (**B**) mouse embryos were cultured for 6 DIV and immunostained for Tuj1 (red). DAPI counterstained nuclei (blue). (**C** and **D**) Double immunostaining of cultured neurons for F-actin (blue) and Tuj1 (red) disclosed the axon shafts and growth cones. (**E** and **F**) Statistical analysis of total neurite length (**E**; control: 165.25 ± 10.52 μm, mutant: 354.19 ± 24.89 μm; $P < 0.0001$, $n = 41$ in the control and $n = 36$ in the mutant) and growth cone areas (**F**; control: 17.48 ± 0.91 μm^2, mutant: 84.89 ± 7.75 μm^2; $P < 0.0001$, $n = 58$ in the control and $n = 40$ in the mutant). (**G**) Protein extracts from E13.5 ventral horns of cervical spinal segments was subjected to western blots using anti-EB3 and β-III tubulin (tubulin). There was a dramatic increase of EB3 in the mutant compared to the control (control: 0.99 ± 0.09, mutant: 1.35 ± 0.01; $P < 0.05$, $n = 3$ animals in each group). *$P < 0.05$; ****$P < 0.0001$; Student's *t*-test.

213 ± 16.6 versus 56 ± 3.5 NMJs/muscle in mutant and control, respectively; $n = 3$ animals in each group; $P < 0.001$). Intriguingly, in cholinergic receptor clusters (labelled by α-BT) of intact biceps, a higher number of axonal terminals showed overgrowth in the mutants (Fig. 4E; 4/52 in control and 17/32 in mutant; $P < 0.01$; chi-square test). On Day 56 post-surgery, EMG recording of biceps showed a higher peak–peak amplitude value on the injured side and an increase of the peak ratio (injured to intact sides) in the mutants compared to the controls, whereas on the intact side, there were no significant differences of EMG amplitude and latencies between the two groups (Fig. 4G–I).

To assess axon regeneration, musculocutaneous nerves collected 56 days after root avulsion/reimplantation were examined by Toluidine Blue staining of plastic sections (Fig. 5A) and by electron microscopy (Fig. 5B). On uninjured sides, total axon numbers were comparable in both groups (Fig. 5A, C and D). However, in electron microscope images, the packing of axons was remarkably denser in the mutant than in the control (Fig. 5B, left two panels). An increase of total axon numbers on the injured sides and of the ratio of injured to intact sides was found in the mutants compared to controls (Fig. 5C and D). In *Celsr2* cKO animals, ChAT immunolabelling of C6 spinal segments showed that more spinal motor neurons survived after root avulsion/reimplantation than in control mice, with increased ChAT-positive cells and higher operated/intact ratio (Supplementary Fig. 3A and B). Thus, our *in vivo* experiments also indicate that *Celsr2* inactivation contributes to neural repair and functional recovery after injury.

CELSR2 knockdown promotes axon growth and fasciculation of spinal motor neurons in humans

To test whether CELSR2 has similar effects in humans as in mice, we used lentiviral vectors encoding *CELSR2* shRNA to knockdown *CELSR2*, and evaluated their efficacy by transfecting cultured motor neurons from WPC7 human embryos. Three different CELSR2-shRNA were compared (Supplementary Fig. 4) and the most efficient one was selected for study. Three days after transfection, *CELSR2* mRNA level was 28% of the controls (using RT-qPCR, Supplementary Fig. 4A) and the protein was 23% of the controls (western blots, Supplementary Fig. 4B and C). Spinal motor neuron explants from WPC7–8 human embryos were cultured and infected with CELSR2 shRNA or scrambled shRNA lentivirus. After

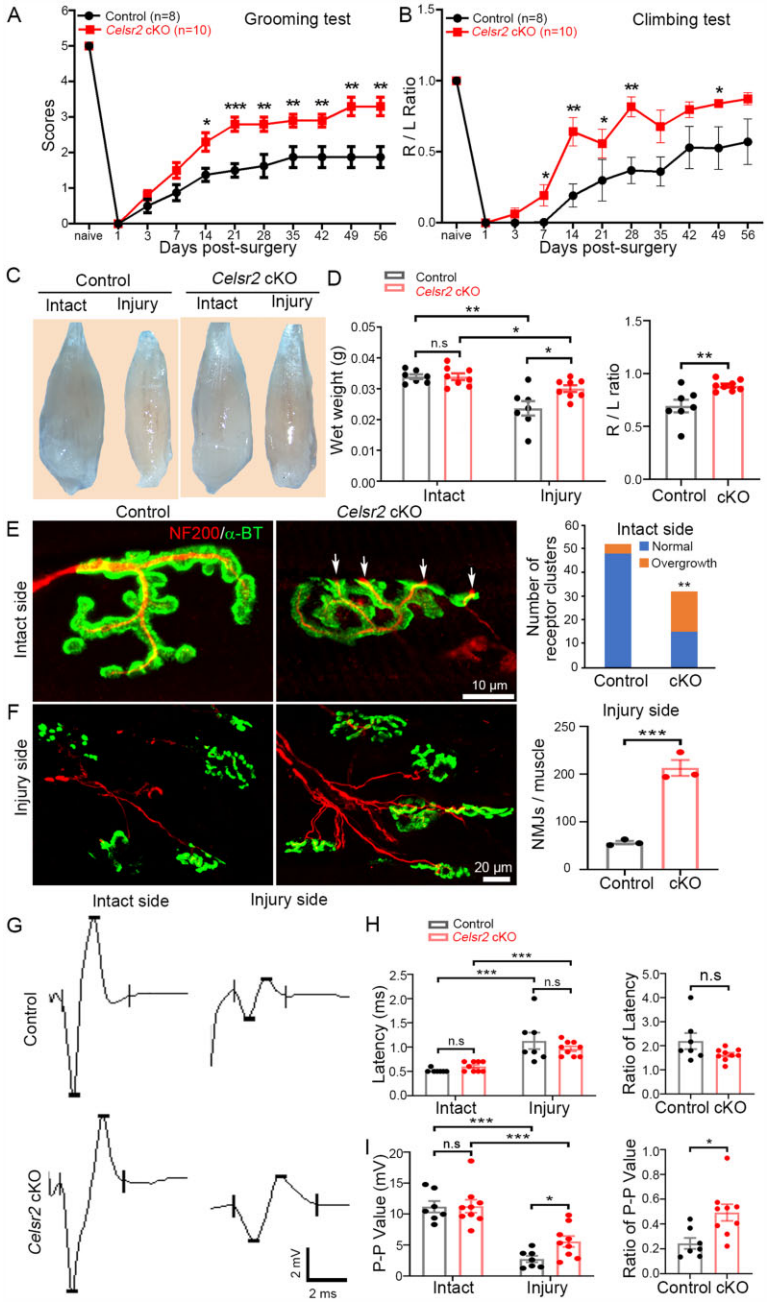

Figure 4 *Celsr2* cKO in spinal motor neurons improves functional recovery and NMJ formation after root avulsion/reimplantation. (**A** and **B**) After root avulsion/reimplantation, the function of the affected forelimb was assessed using the grooming (**A**) and climbing test (**B**). Scores were significantly higher in *Celsr2* cKO (*Isl1-Cre*; *Celsr2*$^{f/-}$) compared to littermate controls (*Celsr2*$^{f/-}$) at Days 14, 21, 28, 35, 42, 49 and 56 post-injury. During the climbing test, usage of injured (R) and intact (L) forelimbs was compared; the R/L ratio was increased in the *Celsr2* cKO. $^{*}P < 0.05$; $^{**}P < 0.01$; Student's *t*-test. (**C** and **D**) Biceps collected 56 days after injury were more atrophic on the injured than the intact side, in both mutant and control mice (**C**). Muscle wet weight on the intact side was comparable in both groups, whereas it was higher on the injured side in mutants versus controls, as reflected by the increased the R/L ratio (injured side to intact side) (**D**). Wet weight, control: 0.0339 ± 0.0008 g, mutant: 0.0339 ± 0.0011 g on the intact side, $P < 0.05$; control: 0.0237 ± 0.0024 g, mutant: 0.0300 ± 0.0010 g on the injured side, $P < 0.05$; the R/L ratio: 0.69 ± 0.06 and 0.89 ± 0.02 in the control and the mutant, respectively, $P < 0.01$. $^{*}P < 0.05$; $^{**}P < 0.01$; Student's *t*-test; $n = 7$ in the control and $n = 8$ in the mutant. (**E** and **F**) NMJs were examined using anti-NF200 and anti-α-BT double staining 56 days post-surgery. On intact sides (**E**), several cholinergic receptor clusters showed axonal terminals overgrowth in *Celsr2* cKO (17/32; indicated by arrows), but rarely in the control (4/52). On injury sides (**F**), there were more numerous growing axons and NMJs in the mutant than in the control (control: 56.33 ± 3.53, mutant: 213.00 ± 16.56 NMJs/muscle, $P < 0.001$, $n = 3$ animals in each group). $^{**}P < 0.01$; $^{***}P < 0.001$; Student's *t*-test for NMJ number comparison and chi-square for receptor cluster comparison. (**G–I**) EMG of biceps was recorded 56 days post-surgery (**G**). The latencies were increased after injury, with no difference between both groups (**H**; control: 0.514 ± 0.014, mutant: 0.600 ± 0.033 ms on the intact side; 1.129 ± 0.170 ms for control and 1.632 ± 0.083 ms for mutant on the injured side; ratio of latency: 2.195 ± 0.335 and 1.632 ± 0.083 in the control and the mutant, respectively; $P > 0.05$ in all comparisons). Denervation resulted in a significant decrease of the peak–peak amplitude in both groups, but the amplitudes and the ratio of the injured to the intact muscle was significantly higher in the mutant compared to the control (**I**; control: 11.182 ± 0.923 mV, mutant: 11.269 ± 1.055 mV on the intact side, $P > 0.05$; control: 2.740 ± 0.523 mV, mutant: 5.572 ± 0.873 mV on the injured side, $P < 0.05$; ratio: 0.244 ± 0.044 and 0.492 ± 0.067 in the control and the mutant, respectively, $P < 0.05$). $^{*}P < 0.05$; $^{**}P < 0.01$; $^{***}P < 0.001$; n.s, not significant; Student's *t*-test; $n = 7$ in the control and $n = 9$ in the mutant.

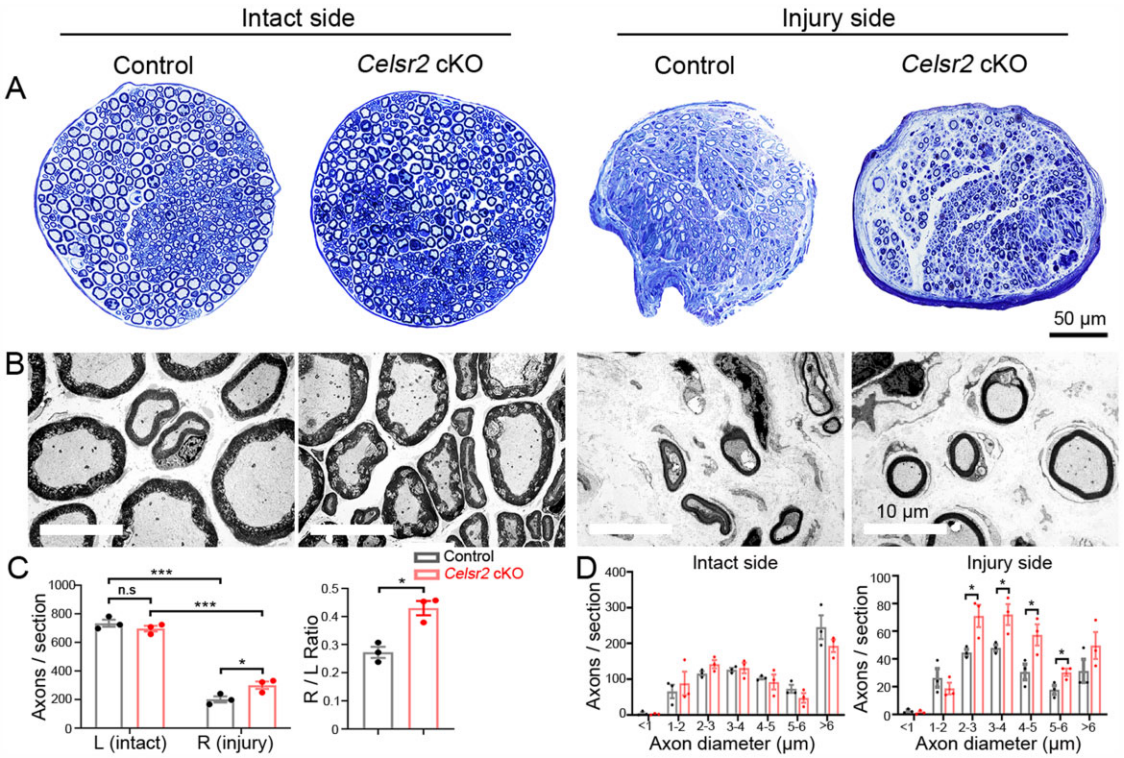

Figure 5 Improved axon regeneration in *Celsr2* cKO mice after root avulsion/reimplantation. (**A**) Toluidine Blue staining of musculocutaneous nerves from intact and injured sides 56 days after root avulsion/reimplantation. (**B**) Electron microscope images of musculocutaneous nerves from intact and injured sides. On the intact side, axons were more closely packed in the mutant than in the control. (**C** and **D**) Statistical analysis showed that axon number was comparable on the intact side in the two genotypes but higher in the mutant on the injured side (**C**; control: 734.0 ± 24.8, mutant: 696.3 ± 20.2 axons/section on the intact side, $P > 0.05$; control: 201.0 ± 21.5, mutant: 300.3 ± 25.8 axons/section on the injured side, $P < 0.05$; the ratio: 0.244 ± 0.044 and 0.492 ± 0.067, $P < 0.05$; $n = 7$ in the control and $n = 9$ in the mutant). The ratio of the injured to the intact side (R/L) was higher in the mutant (**C**; control: 0.27 ± 0.02, mutant: 0.43 ± 0.03, $P < 0.05$; $n = 3$ in each group). The distribution of axons according to their diameter showed no differences in the two genotypes on the intact side and an increased number of axons with 2–6 μm diameter on the operated side in the mutant relative to the control (**D**). *$P < 0.05$; **$P < 0.01$; ***$P < 0.001$; n.s, not significant; Student's *t*-test.

5 DIV, cultured explants were immunostained with anti-ChAT and anti-Tuj1 antibodies. In both groups, lentivirus-tagged green fluorescent protein (GFP) labelled cells in the explants and some labelled neurons migrated out of the explants (Supplementary Fig. 5A and E). ChAT- and Tuj1-immunoreactivity were consistently co-localized in the explants and outgrowing axons (Supplementary Fig. 5B–D and F–H), indicating that growing axons stemmed from motor neurons. Compared with mouse, the human explants developed faster, and the area covered by growing axons was much larger after 5 DIV (Fig. 6A–D) than that in mouse after 6 DIV (Fig. 2B and E). Intriguingly, in the *CELSR2*-shRNA group, growing axons often gathered to form circles (11/27; Fig. 6C, C′ and G) and some aggregated into large bundles (Fig. 6D and D′). We measured the maximal covering area and axonal length in anti-Tuj1 immunostaining preparations. Statistical analysis confirmed a significant increase in both parameters in *CELSR2*-shRNA transfected explants compared with those transduced by scrambled shRNA (Fig. 6E and F; three human embryos; 24 and 23 explants in the CELSR2-shRNA and the control, respectively; $P < 0.0001$). In addition, larger axonal bundles (>8 μm in diameter) were significantly increased after *CELSR2*-shRNA infection (Fig. 6H; $P < 0.0001$).

In human primary motor neuron culture, lentivirus-tagged GFP labelled neuronal soma and neurites exactly like Tuj1-immunostaining (Fig. 7A and B). Total neurite length was increased in *CELSR2*-shRNA transfected neurons at 5 DIV (Fig. 7C; two WPC7 and one WPC8 human embryos, 43 and 36 neurons from the control and the *CELSR2*-shRNA transfection, respectively; $P < 0.0001$). GFP also filled growth cones which were visualized by anti-F-actin immunostaining (Fig. 7D and E). The growth cone area was considerably larger in the *CELSR2*-shRNA than the control group (Fig. 7F; $P < 0.0001$). In 5-DIV CELSR2-shRNA transfected neurons, EB3 protein levels were significantly higher than in controls (Fig. 7G; three independent experiments; $P < 0.05$). In 19-DIV cultured human motor neurons, the peak of potassium-induced intracellular calcium was more elevated in CELSR2-shRNA transfected neurons than in controls (Fig. 7H; $P < 0.05$). Therefore, knocking down *CELSR2* in human preparations similarly promotes axonal regeneration and fasciculation as the findings in mouse.

Celsr2 inactivation results in increased Rac1/Cdc42 and JNK/c-Jun signalling

Small Rho family GTPases Cdc42 and Rac1 are critical modulators of cytoskeleton organization, with their GTP-bound active form stimulating neurite growth.[32] To determine whether *Celsr2* inactivation is associated with the Cdc42/Rac1 signalling, we studied the expression and/or activity of Cdc42 and Rac1 in spinal samples. The proteins were extracted from adult spinal cords after root avulsion, E13.5 cervical spinal segments or cultured human spinal motor neurons. GTP-bound Rac1 and Cdc42 proteins were pulled down using agarose beads conjugated to the protein binding domain of PAK1 fused to GST, followed by elution and western blot analysis with anti-Rac1 and anti-Cdc42 antibodies. In samples of C5–C7 spinal ventral columns 3 days after C5–C7 root avulsion, total Cdc42 and Rac1 levels were similar in *Celsr2*$^{-/-}$ and control extracts (Fig. 8A and B). However, in *Celsr2*$^{-/-}$ mutants, levels of

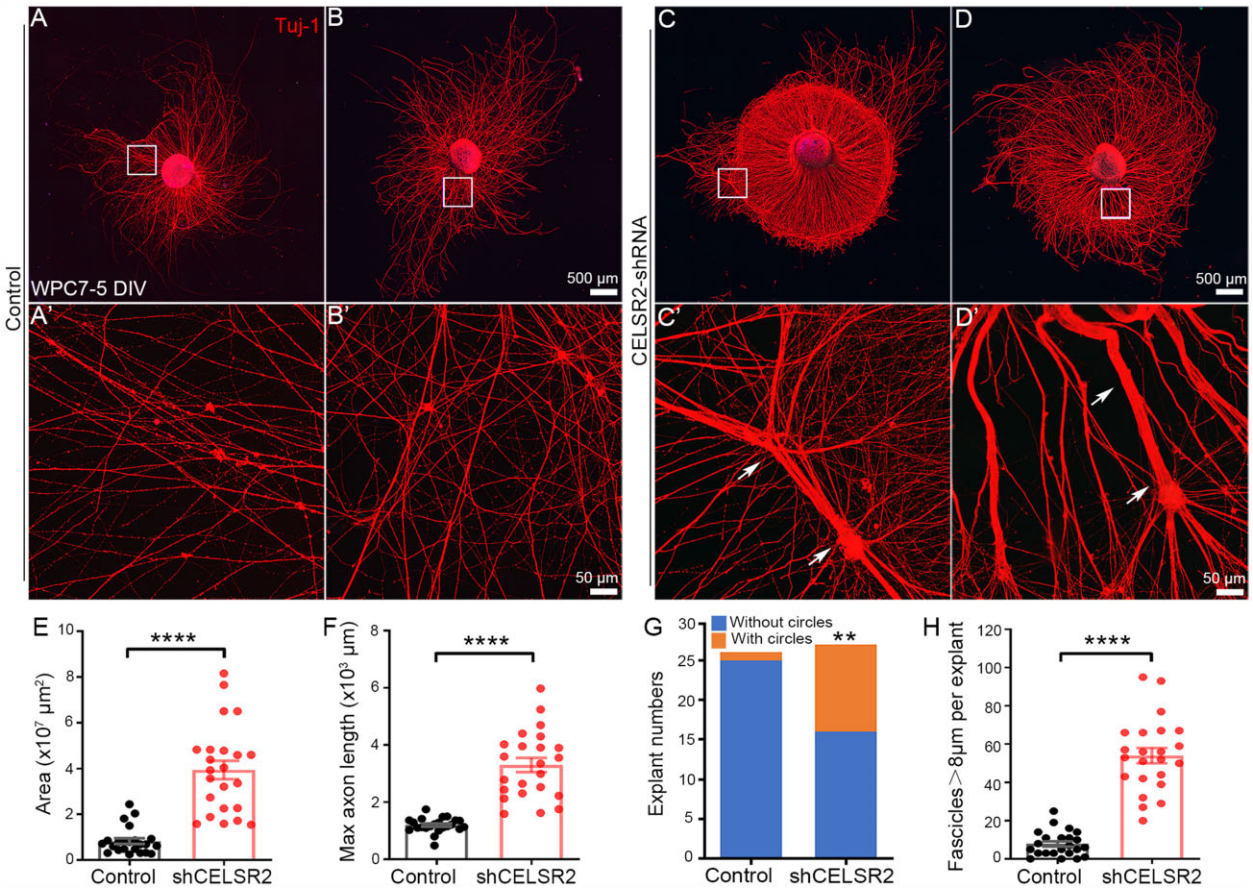

Figure 6 ***CELSR2* knockdown increases axonal regeneration in human embryonic spinal motor explant culture**. (**A**–**D**) Cultured spinal motor neuron explants from WPC7 human embryos were transfected with a CELSR2 scrambled shRNA as control (**A** and **B**) and with CELSR2-shRNA (**C** and **D**). After 5 DIV, cultured explants were immunostained for Tuj1. **A**′, **B**′, **C**′ and **D**′ are enlarged areas from **A**, **B**, **C** and **D**, respectively. Upon CELSR2-shRNA knockdown, growing axons grew in circles (one example indicated in **C**) and formed large axonal bundles (arrows in **C**′ and **D**′). (**E**–**H**) The maximal area in 10^7 μm^2 (**E**; control: 0.82 ± 0.12, CELSR2-shRNA: 3.93 ± 0.40; $P < 0.0001$, $n = 23$ in each group), maximal axon length in 10^3 μm (**F**; control: 1.20 ± 0.05, and CELSR2-shRNA: 3.30 ± 0.25; $P < 0.0001$, $n = 23$ in each group), explants with axons growing into circles (**G**; 1/26 in the control and 11/27 in the CELSR2-shRNA) and the number of large axon bundles (**H**; control : 7.83 ± 1.37, mutant: 53.96 ± 3.98, $P < 0.0001$, $n = 23$ in each group) were significantly increased in the CELSR2-shRNA knockdown explants compared to control. ****$P < 0.0001$; Student's *t*-test (**E**, **F** and **H**). **$P < 0.01$; chi-square test (**G**).

GTP-bound Cdc42 and Rac1 were about 2.2-fold and 1.9-fold of those in controls, respectively (Fig. 8E and F; six animals in each group, samples from two animals were mixed together in the same group, three independent experiments). As JNK and c-Jun are downstream partners regulated by Rac1 and Cdc42 during cytoskeleton reorganization,[33] we estimated their expression using western blots (Fig. 8C and D). There was a significant increase of JNK and c-Jun concentrations in *Celsr2* mutants versus control samples (Fig. 8G and H; six animals in each group, samples from two animals were mixed in the same group, three independent experiments).

In E13.5 mouse ventral spinal samples, the levels of active Cdc42 and Rac1 proteins were also enhanced by 1.55 (Cdc42) and 1.74 (Rac1) fold in *Celsr2*$^-$ mutants compared with control samples, whereas total Cdc42 and Rac1 levels were comparable in two groups (Supplementary Fig. 6A, B, E and F; three independent experiments). In addition, there was a significant increase of JNK and c-Jun concentrations in *Celsr2* mutant versus control samples (Supplementary Fig. 6G and H; three independent experiments; $P < 0.05$). In cultured human spinal motor neurons, *CELSR2*-shRNA transfection remarkably resulted in 1.36- and 2.08-fold increase of GTP-Cdc42 and GTP-Rac1 proteins, respectively, compared with the control, whereas total protein levels were comparable (Supplementary Fig. 7A, B, E and F; proteins from three independent culturing experiments of three human embryos). The levels of JNK and c-Jun were also increased upon *CELSR2* knockdown (Supplementary Fig. 7C, D, G and H).

Discussion

The intrinsic regenerative capacities of the adult CNS in higher animals are very limited, often leading to irreversible functional deficits after injury. Identification of key genes and networks regulating axon regeneration could potentially benefit repair and functional recovery. In this study, we showed that the expression of Celsr2 in adult spinal motor neurons plays an inhibitory role in axon regeneration, through downregulation of the Rac1/Cdc42 and JNK/c-Jun pathways. Inactivation of Celsr2 in cultured human and mouse spinal cord explant and motor neurons dramatically enlarged growth cones and promoted axon outgrowth. Notably, conditional inactivation of *Celsr2* in adult mouse motor neurons significantly improved axon regeneration, motor neuron survival and locomotor recovery after lesion.

Together with its two paralogues Celsr1 and Celsr3, Celsr2 form a small family of adhesion G-protein-coupled receptors. Genetic studies in mice showed that Celsr2 and Celsr3 act synergistically

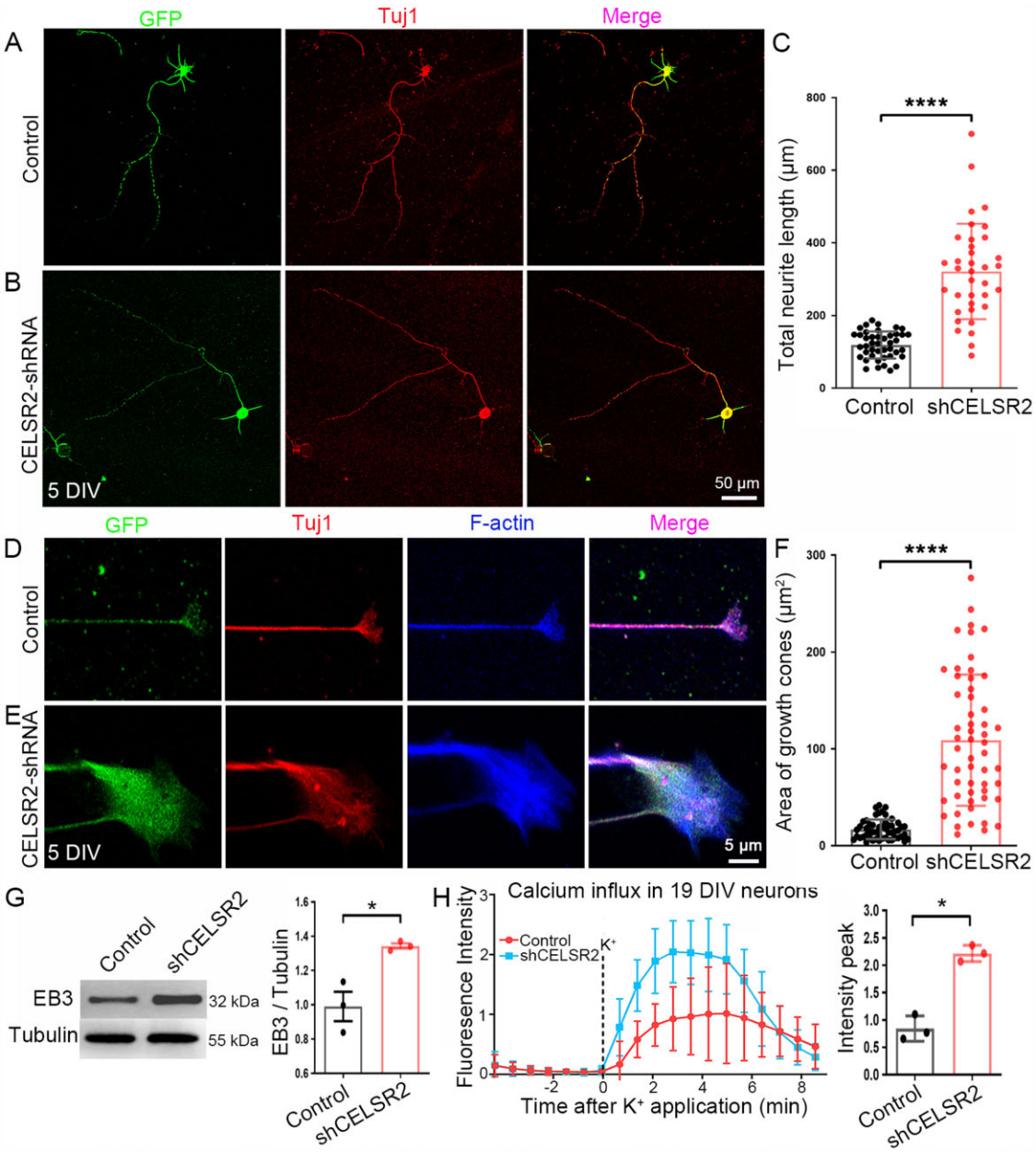

Figure 7 *CELSR2* knockdown promotes axonal growth in primary human spinal motor neuron culture. (**A–C**) CELSR2 scrambled shRNA (**A**, control) and CELSR2-shRNA (**B**) were used to transfect cultured primary spinal motor neurons from WPC7 and WPC8 human embryos. Transfected neurons were visualized by virus-encoded GFP (green). After 5 DIV, neurons were immunostained for Tuj1 (red). GFP- and Tuj1-immunoreactivity overlapped in the somas and neurites as shown in the merged images. A significant increase of total neurite length was observed in CELSR2-shRNA transfected neurons (**C**; in μm, control: 118.70±5.66, CELSR2-shRNA: 321.28±21.90, $P < 0.0001$, $n = 43$ in the control and $n = 36$ in the CELSR2-shRNA). (**D–F**) Double immunostaining for F-actin (blue) and Tuj1 (red) reveal axon shafts and growth cones in control (**D**) and CELSR2-shRNA (**E**) transfected neurons (GFP labelling, green). The growth cone area was significantly increased in CELSR2-shRNA versus control transfected neurons (**F**; control: 16.92±1.40 μm^2, and CELSR2-shRNA: 109.00±9.12, $P < 0.0001$, $n = 52$ in the control and 55 in the CELSR2-shRNA). (**G**) Western blot analysis of 5-DIV cultured neurons with antibodies to EB3 and β-III tubulin (tubulin, reference) showed an increase of EB3 levels in CELSR2-shRNA transfected neurons (control: 0.99±0.09, CELSR2-shRNA: 1.34±0.02, $P < 0.05$, $n = 3$ independent experiments). (**H**) Intracellular calcium influx was evaluated in 19 DIV-cultured neurons by measuring Fluoro-4 AM fluorescence intensity. The curves were drawn from captured images before and after potassium application. There was an increase of the fluorescent peaks in CELSR2-shRNA transfected neurons (control: 0.84±0.13, and CELSR2-shRNA: 2.22±0.09, $P < 0.05$, $n = 3$ independent experiments). *$P < 0.05$; ****$P < 0.0001$; Student's *t*-test.

during neural development, particularly in regulating axon guidance and ependymal cilia biogenesis.[10] In most cases, inactivation of *Celsr2* causes milder embryonic phenotypes than that of *Celsr3*, while joint inactivation generates severe phenotypes that mimic closely those resulting from inactivation of *Fzd3*, a member of the frizzled family of Wnt receptors.[16] Celsr3 can co-immunoprecipitate with Fzd3,[14] and this might explain similarity of mutant phenotypes. Neural specific inactivation of *Rac1* impairs extension of motor axons of the peroneal nerve,[17] a phenotype identical to those observed when *Fzd3* or *Celsr2* and 3 are conditionally inactivated in motor neurons, suggesting Fzd3 and Celsr2 and 3 may upregulate Rac1. However, we found that Celsr2 regulates Rac1/Cdc42 and JNK signalling negatively, rather than positively. A possible explanation is that Wnt/PCP signalling might stimulate the

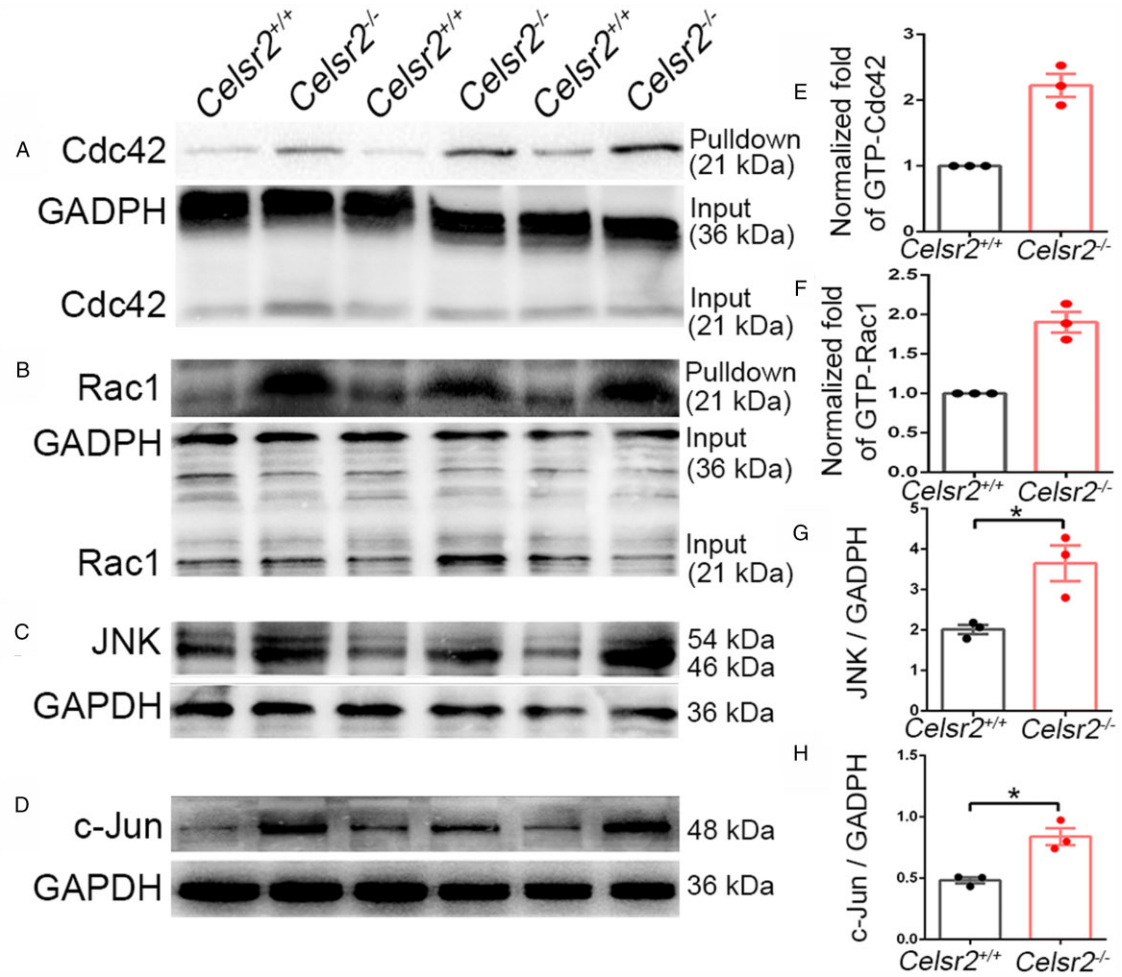

Figure 8 *Celsr2* knockout increases Cdc42/Rac1 and JNK/c-Jun signalling in injured ventral horns. (**A–D**) Western blot analysis of GST-pulldown proteins and samples from spinal ventral columns 3 days after root avulsion, using anti-Cdc42 (**A**), anti-Rac1 (**B**), anti-JNK (**C**), anti-c-Jun (**D**) antibodies. Anti-GADPH antibody was used as reference. (**E–H**) GTP-bound Cdc42 (**E**; control: 1±0, mutant: 2.22±0.17, $P < 0.05$) and Rac1 (**F**; control: 1±0, mutant: 1.90±0.13, $P < 0.05$) proteins, as well as concentrations of JNK (**G**; control: 2.01±0.12, mutant: 3.65±0.44, $P < 0.05$) and c-Jun (**H**; control: 0.48±0.02, mutant: 0.84±0.07, $P < 0.05$) were increased in mutant compared to control samples. *$P < 0.05$; Student's *t*-test; $n = 3$ animals in each group.

Rac1/Cdc42 pathway during embryonic development, while inhibiting the same pathway in adult axon regeneration. In support of this, at least two examples of negative regulation of the Rac1/Cdc42-JNK pathway by Wnt/PCP signalling have been published, namely the effect of Fzd6, the closest paralogue of Fzd3[34] and of Fzd8 working together with Celsr2 in haematopoietic stem cells.[35] The Celsr2 ectodomain is implicated in homophilic interactions[15] and could mediate repulsion between axons, accounting for increased fasciculation upon *Celsr2* inactivation and increased axon packing observed in *Celsr2* cKO musculocutaneous nerves by electron microscopy. In line with this, in *Drosophila*, its orthologue Flamingo mediates homophilic repulsion of homologous neurons at the dorsal midline, and mutations result in formation of neurite tangles and dendrites overgrowth.[36] Celsr2-mediated repulsion might be implicated in cilia organization,[13] motor neuron migration[11] and axon navigation.[14] In corollary, *Celsr2* inactivation may foster the formation of large axon bundles and thereby contribute to axon regeneration and survival of injured neurons. The interaction between peripheral nerves and Schwann cells is also important for axon regeneration.[37] Whether *Celsr2* silencing influences neural regeneration by modulating axon-Schwann cell interactions awaits further investigations.

Previous studies outlined a role of JNK in PCP and noncanonical Wnt signalling, implicating, among others, the Wnt5a ligand and frizzled receptor Fzd6, a close relative of Fzd3.[38–41] Our data are the first indication that Celsr2 acts via the same pathway. Mechanistic links between Frizzled and Rac1/Cdc42 remain incompletely understood but could involve Dishevelled adaptors and formins such as Daam1-2.[42] The Rac1/Cdc42-JNK/c-Jun signalling module is better documented. Cdc42 and Rac1 are two important small GTPases of the Rho family, and their active form regulates actin dynamics in navigating growth cones, promoting axon growth.[32] Downstream of Rac1/Cdc42, the pathway sequentially involves MAP3K mixed lineage kinases such as DLK, as well as MKK7/4 and JNK1-3.[43,44] The cascade is coordinated by docking adaptors such as JIP1/POSH.[45–47] The Rac1/Cdc42—JNK/c-Jun pathway is a 'double-edged sword', with variable, often paradoxical actions. On the one hand, it can mediate neuronal apoptosis upon nerve growth factor deprivation[48] and is implicated in Wallerian axon degeneration.[49] On the other hand, upregulation of c-Jun is correlated with axon regeneration after injury.[50] JNK is necessary for the nuclear translocation of c-Jun to maintain cytoskeletal integrity during axon extension[51] and DLK activation is required for axon regeneration.[52]

Besides upregulating Rac1/Cdc42 signalling, *Celsr2* inactivation also increases expression of the microtubule plus end-binding protein EB3, and stimulates potassium-induced calcium influx. EB3 interacts not only with microtubules, but also with actin filaments,

via drebrin, and those interactions could promote growth cone formation and neurite extension.[27] Similarly, an influx of calcium could activate calcium-/calmodulin-dependent protein kinase II, which regulates F-actin to stimulate growth cone extension during development and after injuries.[53]

Conclusion

Our data uncover a previously unknown role of Celsr2 in the regulation of axon regeneration, via Rac1/Cdc42 and possibly other mechanisms. The fact that concordant data were observed in humans and mice, and in both embryonic and adult axons, strongly suggests that this function of Celsr2 is physiopathologically relevant and that Celsr2 is a potential target to promote neural repair.

Acknowledgements

We wish to thank Meizhi Wang, Lei Shi for technical assistance and Guoliang Chai and Kwok-Fai So for critical comments.

Funding

This work was supported by the following grants: National Natural Science Foundation of China (81971148, L.Z; and 82071261 and 31671067, Y.Q.), Guangzhou Key Projects of Brain Science and Brain-Like Intelligence Technology (20200730009, L.Z), Guangdong grant 'Key technologies for treatment of brain disorders' (2018B030332001, L.Z.), Health and Medical Collaborative Innovation Major Projects of Guangzhou (201803040016–2, L.Z.; 201604046028, L.Z. and K. F. So), Programme of Introducing Talents of Discipline to Universities (B14036), Outstanding Scholar Program of Bioland Laboratory (Guangzhou Regenerative Medicine and Health Guangdong Laboratory; 2018GZR110102002), Guangdong Natural Science Funds for Distinguished Young Scholars (2016A030306001, Y.Q.), Guangdong Province Special Support Program (2015TQ01R837, Y.Q.), Key-Area Research and Development Program of Guangdong Province (2018B030340001) and Pediatrics/Guangzhou Women and Children Medical Center funds (GCP-2019–002).

Competing interests

The authors report no competing interests.

Supplementary material

Supplementary material is available at *Brain* online.

References

1. Liu K, Tedeschi A, Park KK, He Z. Neuronal intrinsic mechanisms of axon regeneration. *Annu Rev Neurosci*. 2011;34:131–152.
2. Mahar M, Cavalli V. Intrinsic mechanisms of neuronal axon regeneration. *Nat Rev Neurosci*. 2018;19(6):323–337.
3. Ruven C, Chan TK, Wu W. Spinal root avulsion: An excellent model for studying motoneuron degeneration and regeneration after severe axonal injury. *Neural Regen Res*. 2014;9(2):117–118.8.
4. Cullheim S, Carlstedt T, Linda H, Risling M, Ulfhake B. Motoneurons reinnervate skeletal muscle after ventral root implantation into the spinal cord of the cat. *Neuroscience*. 1989;29(3):725–733.
5. Carlstedt T, Grane P, Hallin RG, Noren G. Return of function after spinal cord implantation of avulsed spinal nerve roots. *Lancet*. 1995;346(8986):1323–1325.
6. Duraikannu A, Krishnan A, Chandrasekhar A, Zochodne DW. Beyond trophic factors: Exploiting the intrinsic regenerative properties of adult neurons. *Front Cell Neurosci*. 2019;13:128.
7. Havton LA, Carlstedt T. Repair and rehabilitation of plexus and root avulsions in animal models and patients. *Curr Opin Neurol*. 2009;22(6):570–574.
8. Carlstedt T. Perspectives on the treatment of the longitudinal spinal cord injury. *Front Neurol*. 2010;1:11.
9. Goffinet AM, Tissir F. Seven pass Cadherins CELSR1–3. *Semin Cell Dev Biol*. 2017;69:102–110.
10. Tissir F, Goffinet AM. Atypical cadherins Celsr1–3 and planar cell polarity in vertebrates. *Prog Mol Biol Transl Sci*. 2013;116:193–214.
11. Qu Y, Glasco DM, Zhou L, et al. Atypical cadherins Celsr1–3 differentially regulate migration of facial branchiomotor neurons in mice. *J Neurosci*. 2010;30(28):9392–9401.
12. Qu Y, Huang Y, Feng J, et al. Genetic evidence that Celsr3 and Celsr2, together with Fzd3, regulate forebrain wiring in a Vangl-independent manner. *Proc Natl Acad Sci U S A*. 2014;111(29):E2996–3004.
13. Tissir F, Qu Y, Montcouquiol M, et al. Lack of cadherins Celsr2 and Celsr3 impairs ependymal ciliogenesis, leading to fatal hydrocephalus. *Nat Neurosci*. 2010;13(6):700–707.
14. Chai G, Zhou L, Manto M, et al. Celsr3 is required in motor neurons to steer their axons in the hindlimb. *Nat Neurosci*. 2014;17(9):1171–1179.
15. Shima Y, Kawaguchi SY, Kosaka K, et al. Opposing roles in neurite growth control by two seven-pass transmembrane cadherins. *Nat Neurosci*. 2007;10(8):963–969.
16. Hua ZL, Smallwood PM, Nathans J. Frizzled3 controls axonal development in distinct populations of cranial and spinal motor neurons. *Elife*. 2013;2:2:e01482.
17. Hua ZL, Emiliani FE, Nathans J. Rac1 plays an essential role in axon growth and guidance and in neuronal survival in the central and peripheral nervous systems. *Neural Dev*. 2015;10:21.
18. Tissir F, Goffinet AM. Expression of planar cell polarity genes during development of the mouse CNS. *Eur J Neurosci*. 2006;23(3):597–607.
19. Hern WM. Correlation of fetal age and measurements between 10 and 26 weeks of gestation. *Obstetr Gynecol*. 1984;63(1):26–32.
20. Wang L, Marquardt T. Direct live monitoring of heterotypic axon–axon interactions *in vitro*. *Nat Protoc*. 2012;7(2):351–363.
21. Matsunaga M, Hatta K, Nagafuchi A, Takeichi M. Guidance of optic nerve fibres by N-cadherin adhesion molecules. *Nature*. 1988;334(6177):62–64.
22. Jaworski A, Tessier-Lavigne M. Autocrine/juxtaparacrine regulation of axon fasciculation by Slit-Robo signaling. *Nat Neurosci*. 2012;15(3):367–369.
23. Bertelli JA, Mira JC. Behavioral evaluating methods in the objective clinical assessment of motor function after experimental brachial plexus reconstruction in the rat. *J Neurosci Methods*. 1993;46(3):203–208.
24. Ding Y, Qu Y, Feng J, et al. Functional motor recovery from motoneuron axotomy is compromised in mice with defective corticospinal projections. *PLoS One*. 2014;9(7):e101918.
25. Starkey ML, Barritt AW, Yip PK, et al. Assessing behavioural function following a pyramidotomy lesion of the corticospinal tract in adult mice. *Exp Neurol*. 2005;195(2):524–539.
26. Han Q, Cao C, Ding Y, et al. Plasticity of motor network and function in the absence of corticospinal projection. *Exp Neurol*. 2015;267:194–208.
27. Geraldo S, Khanzada UK, Parsons M, Chilton JK, Gordon-Weeks PR. Targeting of the F-actin-binding protein drebrin by the microtubule plus-tip protein EB3 is required for neuritogenesis. *Nat Cell Biol*. 2008;10(10):1181–1189.

28. Gasperini RJ, Pavez M, Thompson AC, et al. How does calcium interact with the cytoskeleton to regulate growth cone motility during axon pathfinding? *Mol Cell Neurosci*. 2017;84: 29–35.
29. Pfaff SL, Mendelsohn M, Stewart CL, Edlund T, Jessell TM. Requirement for LIM homeobox gene Isl1 in motor neuron generation reveals a motor neuron-dependent step in interneuron differentiation. *Cell*. 1996;84(2):309–320.
30. Song MR, Sun Y, Bryson A, Gill GN, Evans SM, Pfaff SL. Islet-to-LMO stoichiometries control the function of transcription complexes that specify motor neuron and V2a interneuron identity. *Development*. 2009;136(17):2923–2932.
31. Fournier HD, Mercier P, Menei P. Repair of avulsed ventral nerve roots by direct ventral intraspinal implantation after brachial plexus injury. *Hand Clin*. 2005;21(1):109–118.
32. Samuel F, Hynds DL. RHO GTPase signaling for axon extension: Is prenylation important? *Mol Neurobiol*. 2010;42(2): 133–142.
33. Hall A. Rho GTPases and the control of cell behaviour. *Biochem Soc Trans*. 2005;33(Pt 5):891–895.
34. Abidin BM, Owusu Kwarteng E, Heinonen KM. Frizzled-6 regulates hematopoietic stem/progenitor cell survival and self-renewal. *J Immunol*. 2015;195(5):2168–2176.
35. Sugimura R, He XC, Venkatraman A, et al. Noncanonical Wnt signaling maintains hematopoietic stem cells in the niche. *Cell*. 2012;150(2):351–365.
36. Gao FB, Kohwi M, Brenman JE, Jan LY, Jan YN. Control of dendritic field formation in *Drosophila*: The roles of flamingo and competition between homologous neurons. *Neuron*. 2000;28(1): 91–101.
37. Wilson ER, Della-Flora Nunes G, Weaver MR, Frick LR, Feltri ML. Schwann cell interactions during the development of the peripheral nervous system. *Dev Neurobiol*. 2021;81(5):464–489.
38. Cheyette BN, Waxman JS, Miller JR, et al. Dapper, a Dishevelled-associated antagonist of beta-catenin and JNK signaling, is required for notochord formation. *Dev Cell*. 2002;2(4):449–461.
39. Lutze G, Haarmann A, Demanou Toukam JA, Buttler K, Wilting J, Becker J. Non-canonical WNT-signaling controls differentiation of lymphatics and extension lymphangiogenesis via RAC and JNK signaling. *Sci Rep*. 2019;9(1):4739.
40. Yamanaka H, Moriguchi T, Masuyama N, et al. JNK functions in the non-canonical Wnt pathway to regulate convergent extension movements in vertebrates. *EMBO Rep*. 2002;3(1):69–75.
41. Yang Y, Mlodzik M. Wnt-Frizzled/planar cell polarity signaling: Cellular orientation by facing the wind (Wnt). *Annu Rev Cell Dev Biol*. 2015;31:623–646.
42. Habas R, Dawid IB, He X. Coactivation of Rac and Rho by Wnt/Frizzled signaling is required for vertebrate gastrulation. *Genes Dev*. 2003;17(2):295–309.
43. Jin Y, Zheng B. Multitasking: Dual leucine zipper-bearing kinases in neuronal development and stress management. *Annu Rev Cell Dev Biol*. 2019;35:501–521.
44. Schellino R, Boido M, Vercelli A. JNK signaling pathway involvement in spinal cord neuron development and death. *Cells*. 2019; 8(12):1576.
45. Kukekov NV, Xu Z, Greene LA. Direct interaction of the molecular scaffolds POSH and JIP is required for apoptotic activation of JNKs. *J Biol Chem*. 2006;281(22):15517–15524.
46. Nihalani D, Meyer D, Pajni S, Holzman LB. Mixed lineage kinase-dependent JNK activation is governed by interactions of scaffold protein JIP with MAPK module components. *EMBO J*. 2001;20(13):3447–3458.
47. Xu Z, Kukekov NV, Greene LA. POSH acts as a scaffold for a multiprotein complex that mediates JNK activation in apoptosis. *EMBO J*. 2003;22(2):252–261.
48. Xu Z, Maroney AC, Dobrzanski P, Kukekov NV, Greene LA. The MLK family mediates c-Jun N-terminal kinase activation in neuronal apoptosis. *Mol Cell Biol*. 2001;21(14):4713- 4724.
49. Miller BR, Press C, Daniels RW, Sasaki Y, Milbrandt J, DiAntonio A. A dual leucine kinase-dependent axon self-destruction program promotes Wallerian degeneration. *Nat Neurosci*. 2009; 12(4):387–389.
50. Raivich G, Bohatschek M, Da Costa C, et al. The AP-1 transcription factor c-Jun is required for efficient axonal regeneration. *Neuron*. 2004;43(1):57–67.
51. Chang L, Jones Y, Ellisman MH, Goldstein LS, Karin M. JNK1 is required for maintenance of neuronal microtubules and controls phosphorylation of microtubule-associated proteins. *Dev Cell*. 2003;4(4):521–533.
52. Nix P, Bastiani M. DLK: The "preconditioning" signal for axon regeneration? *Neuron*. 2012;74(6):961–963.
53. Xi F, Xu RJ, Xu JH, et al. Calcium/calmodulin-dependent protein kinase II regulates mammalian axon growth by affecting F-actin length in growth cone. *J Cell Physiol*. 2019;234(12): 23053–23065.